Applied Catalysis B: Environmental 300 (2022) 120688

Contents lists available at ScienceDirect

Applied Catalysis B: Environmental

journal homepage: www.elsevier.com/locate/apcatb

Selective photocatalytic oxidation of gaseous ammonia at ppb level over Pt and F modified TiO_2

Yajie Shu [a,b], Jian Ji [a], Ming Zhou [c], Shimin Liang [a], Quan Xie [a], Sitan Li [a], Biyuan Liu [a], Jiguang Deng [d], Jianping Cao [a], Shengwei Liu [a,*], Haibao Huang [a,*]

[a] School of Environmental Science and Engineering, Guangdong Provincial Key Laboratory of Environmental Pollution Control and Remediation Technology, Sun Yat-sen University, Guangzhou 510006, PR China
[b] Key Laboratory of Materials Physics, Centre for Environmental and Energy Nanomaterials, Anhui Key Laboratory of Nanomaterials and Nanotechnology, CAS Center for Excellence in Nanoscience, Institute of Solid State Physics, Chinese Academy of Sciences, Hefei, Anhui 230031, PR China
[c] Centre for Clean Environment and Energy, Gold Coast Campus, Griffith University, QLD 4222, Australia
[d] College of Environmental and Energy Engineering, Beijing University of Technology, Beijing 100124, PR China

ARTICLE INFO

Keywords:
Selective photocatalytic oxidation
F or Pt modification
NH_3 removal
NO_x byproduct
N_2

ABSTRACT

Ammonia (NH_3) as an important precursor to form atmospheric fine particles and secondary inorganic aerosols, should be strictly controlled. Photocatalysis has provided a facile and an effective way to eliminate NH_3 pollution under mild conditions, whereas the undesirable products, such as NO, NO_2 would be generated during the reaction and the mechanism remains unclear. In this study, F or Pt modified TiO_2 were explored to reduce the formation of NOx during photocatalytic oxidation of low-concentration NH_3, and its photocatalytic activity, selectivity and mechanism of NH_3 conversion were systematically studied. Results indicate that surface fluorination on TiO_2 contribute to the reduction of noxious NO_x, especially for NO_2, since the modified TiO_2 achieved enhanced adsorption of NH_3 and strong electron-trapping ability, which can retard the recombination of photogenerated electrons and holes. In addition, the deposition of Pt could further extend the lifetime of the electron-hole pairs by strongly capture the electron, and enhance the oxidation of NH_3 into nitrates and nitrites species. From the *in-situ* DRIFT spectroscopy and XPS results, we can deduce that reactive amino radical ($\bullet NH_2$) would be formed on TiO_2 under photoirradiation after the adsorption of NH_3 on Lewis acid cites. The formed $\bullet NH_2$ can react with reactive oxygen species in the presence of H_2O, and produce NO_x and HNO_x. By both enhancing the adsorption of NH_3 and separation efficiency of electron-hole pairs, the presence of F and Pt modification on the TiO_2 changes the photocatalytic pathway of NH_3 conversion. The proposed selective oxidation mechanism may offer a novel insight into the photocatalytic oxidation of atmospheric NH_3 on other metal oxide with surface modification and can be broadly employed in air pollution control in indoor environments.

1. Introduction

Ammonia (NH_3), a predominant alkaline air pollutant, is intensively discharged from agricultural activities [1], wastewater treatment [2], refuse landfill [3] and motor vehicle exhaust [4,5], as well as indoor release from decorative materials [6], toilet and kitchen garbage [7]. In recent years, NH_3 has attracted increasing attention [8–10] due to its active participation in atmospheric chemistry reaction with acidic gases (*e.g.*, SO_2 and NO_x) [11], leading to the formation of secondary inorganic aerosols (SIA, *e.g.*, $(NH_4)_2SO_4$ and NH_4NO_3). Nevertheless, they typically make up from 20% to 80% of $PM_{2.5}$, severely degrading regional air quality and posing a great threat to the atmospheric environment. Besides, as an universal pollutant in indoor environment, NH_3 has a strong pungent odor which is hazardous and detrimental to the public health and safety [12]. According to the U.S. Occupational Safety and Health Administration and British Health and Safety Executive, the recommended airbone NH_3 exposure limit is 25 ppm averaged over an 8 h period and 35 ppm over any 15 min work period. Indoor Air Quality Standard (IAQS) in China has set limits on indoor NH_3 concentration at a level of less than 0.2 mg/m^3 (0.152 ppm). For these reasons, it is highly necessary to develop the efficient techniques to eliminate the ignorable gaseous NH_3 [13,14]. However, the concentration of NH_3 in the

* Corresponding authors.
E-mail addresses: liushw6@mail.sysu.edu.cn (S. Liu), seabao8@gmail.com (H. Huang).

https://doi.org/10.1016/j.apcatb.2021.120688
Received 10 July 2021; Received in revised form 25 August 2021; Accepted 3 September 2021
Available online 9 September 2021

atmosphere and indoor environment is generally very low, and the emission sources are mostly irregular and unrestrained [49], which make it hard for the effective removal. Apart from the methods of absorption [15], biological conversion [16] and thermal combustion [17], selective catalytic oxidation (SCO) of ammonia and the selective catalytic reduction (SCR) of NO_x with ammonia have been widely studied [18–21]. Nevertheless, SCO/SCR technology are often used for the removal of high-concentration NH_3 from industry, and still suffer from unclear oxidation mechanism and undesirable products [22].

Photocatalytic oxidation of NH_3 has been considered as an available and simple method due to its facile and mild conditions [23,24]. Among various photocatalysts, TiO_2 is considered as the most popular materials due to its abundance, cheapness, low toxicity, chemical and photo-stability, and strong photo-oxidative ability [25–27]. Yamazoe et al. [28] investigated the photo-SCO performance over various commercial TiO_2 in a conventional fixed bed flow system and found that the photo-SCO activity correlated to the amount of chemisorbed NH_3 and the oxygen anion radical species. However, TiO_2 still suffers from low photocatalytic efficiency due to the fast recombination rate of photo-induced charge carriers. Besides, most researches regarding the SCO or SCR processes focused on the NH_3 with high concentration, while the activity and the underlying oxidation process for NH_3 over photocatalysts would be quite different when it was involved in low concentration. Kebede et al. [29] found that the atmospherically relevant levels of NH_3 would become an important source of NO and NO_2 by photochemically oxidizing NH_3 into NO_x over TiO_2, which is a potentially precursor to atmospheric ozone, and rendering the degradation process an ineffective removal pathway.

The surface modification over photocatalysts has an effect on its physical-chemical and photo-chemical properties [30,31], which would enhance the photo-SCO performance of NH_3. Li et al. [32] prepared ultrafine TiO_2 encapsulated in the nitrogen-doped porous carbon framework to effectively degrade NH_3 gas under light irradiation. Deng et al. [33] found that MnO_x/TiO_2 with preferentially exposed {001} facet showed a better SCR performance of NO and high N_2 selectivity at low temperature. Chen et al. [34] found that the surface fluorination increased the SCO activity of NH_3 over TiO_2 by drawing the photo-generated holes to the {001} facet and reducing the electron-hole recombination rate. However, the relationship between the surface fluorination and the degradation pathway of NH_3 has not been fully understood. In addition, the undesirable products such as NO, NO_2 and N_2O are extensively generated from NH_3 oxidation over most catalysts [35]. It is highly necessary to develop novel photocatalysts to avoid such toxic products and increase the selectivity of NH_3 oxidation to mildly oxidized products - innocuous N_2 [36]. Fundamental knowledge of the relationship among the structural properties including surface modification over catalysts, the oxidative intermediates and products, and the mechanism of NH_3 oxidation still needs to be studied in depth.

Herein, to systematically study the photocatalytic activity and selectivity of NH_3 conversion at ppb level and gain more fundamental insights into the oxidation mechanism, the roles of non-metal/metal modification over photocatalysts were well explored in this work. We take TiO_2 nanosheet as our model catalyst to get a further understanding of facet engineering and instruction for the shape-controlled strategies. And discuss the effects of the typical surface modification-fluorination and Pt deposition in relation with their synergistic effect over NH_3 photooxidation. The oxidation mechanism were explored by *in-situ* DRIFT and the catalysts were characterized to obtain the physiochemical properties. To the best of our knowledge, no attempt has been made to elucidate the photocatalytic oxidation mechanism of low concentration NH_3 over surface modified TiO_2 and its structure-activity relationship involving with band gap energies, adsorptive capacities, and electron-hole recombination efficiencies. The proposed mechanism can offer a novel insight for the design of efficient catalysts and its further applications in photocatalytic oxidation of NH_3 pollutant in indoor environments.

2. Experimental

2.1. Preparation of catalysts

Commercial TiO_2 used in this study were supplied from Degussa (P25, 99.5%). The HF modified TiO_2 catalyst were initially prepared *via* simple hydrothermal method as reported in the previous literature [37] with 4 mL HF and 0 mL HF and the obtained catalyst is named as TF4 and TF0, respectively.

In order to defluorinate the TF4 catalyst, the obtained TF4 was subsequently washed with 0.1 M NaOH solution (labeled as TF4-NaOH), or calcinated at 500 ℃ in air (labeled as T500), respectively.

For comparison, the surface fluorination of TF0 (F-TF0) and P25 (F-P25) were obtained by NaF impregnation method.

Pt-loaded TiO_2 was obtained using a photochemical reduction deposition method [38]. Typically, 0.5 g of TiO_2 powders (P25, TF4 and TF0) were dispersed with H_2PtCl_6 solution in a 100 mL aqueous suspension under stirring. The suspension was subsequently irradiated for 1 h with a 300 W Xe lamp (PLS-SXE300) for photodeposition. The solid samples were washed with DI water and collected by centrifugation and drying in an oven at 80 °C for 12 h.

All the samples (0.1 g) were well dispersed in 10 mL ethanol by ultrasonic technique for 10 min, and the mixed paste was treated to spread on the glass substrate. The as-prepared sample was then dried at 60 °C for 1 h to remove residual ethanol.

2.2. Materials characterization

The morphology of the synthesized catalysts were characterized by means of scanning electron microscopy (SEM, Quanta 400 FEG), Transmission electron microscopy (TEM) and High resolution transmission electron microscopy (HRTEM) obtained on a JEOL JEM-2100F with acceleration voltage of 200 kV. X-ray powder diffraction (XRD) measurement was conducted on a Smartlab-3KW (Rigaku Ltd.) diffractometer with Cu Kα radiation (λ = 0.154056 nm). N_2 adsorption−desorption data were collected on a Tristar II 3020 M (Micromeritics) instrument. The specific surface area was calculated by the Brunauer-Emmett-Teller (BET) method. The pore volume was obtained from the adsorption isotherm according to the Barrett-Joyner-Halenda (BJH) model. X-ray photoelectron spectra (XPS, Thermo-ESCALAB 250XI) were carried out on an X-ray photoelectron spectrometer with Al Kα radiation. Absorption spectra and light transmittance were measured through a UV-Vis diffuse reflection spectral system (UV-2600) over a range of 200–800 nm using $BaSO_4$ as reference.

2.3. Catalytic activity measurements

The measurement of NH_3 degradation was performed in a fixed-bed continuous-flow reactor as shown in the supporting information (Fig. S1). The feed gas containing around 820 ppb NH_3, 5% O_2, and N_2 as the balance gas and water vapor were introduced into the reactor with a flow rate of 1 L/min at a relative humidity (RH) of 50%. The NH_3 concentration, humidity and gas flow were controlled by the mass flow controllers. 0.1 g prepared catalyst was taken in the test, corresponding to a gas hourly space velocity (GHSV) of 36,000,000 mL/(g_{cat}·h). The concentrations of NH_3, NO, NO_2 and NO_x was measured by NH_3 analyzer (17i , Thermo Fisher Nicolet). The test temperature was around 25 °C. Before each test, we would carry out a 2 h dark adsorption with a continuous stream of NH_3 in humidified air to achieve NH_3 adsorption-desorption equilibrium.

The *in-situ* diffuse reflectance infrared Fourier transform (*in-situ* DRIFT) spectroscopy were carried out on a FTIR spectrophotometer (Nicolet iS10, Thermo Fisher Scientific, USA) with an *in-situ* cell. All samples were pre-purged with Ar for 1 h at room temperature before switching to the feed gas. All spectra were acquired with a resolution of 8 cm^{-1} for 16 scans, over a wavenumber range between 750 and 4000

cm^{-1}.

3. Results and discussion

3.1. Photocatalytic oxidation of NH_3

Fig. 1 shows the photocatalytic oxidation of NH_3 and the outlet concentrations of formed NO and NO_2 over various TiO_2 (P25, TF0 and TF4) in the flow reactor system under 300 W Xe lamp. Before the light was turned on, a continuous stream of ~820 ppb NH_3 in humidified air (50% RH) was fed into the process and flowed through the surface of samples in the dark for 2 h to achieve NH_3 adsorption-desorption equilibrium. It can be seen that different TiO_2 exhibited different NH_3 adsorption-desorption ability. The prepared TiO_2 (TF0, TF4) had the similar NH_3 adsorption-desorption equilibrium concentration at around 600 ppb, while P25 owned a higher concentration of 700 ppb. When the light was on, NH_3 concentration of all the samples went through a increase due to the strong heat of the light and then dropped to around 420 ppb in 150 min. Specifically, the sharp increase of P25 was more intense than the other two samples, indicating the weak bonding of NH_3 with the P25.

Even though the residual NH_3 over P25, TF0 and TF4 was quite close (420 ppb of P25, 450 ppb of TF0 and 400 ppb of TF4, respectively), the formed NO and NO_2 showed different trends. Seen from Fig. 1(b and c), all the samples exposed NH_3 were unreactive in the dark but generated NO_x when being irradiated. TF4 got the lowest NO and NO_2 outlet concentration with 12 ppb, far less than that of P25 (12 ppb and 100 ppb, respectively) and TF0 (30 ppb and 175 ppb, respectively), suggesting that TF4 would have a more effective pathway of decomposing NH_3. It is interesting to find that the concentration of outlet NO_2 was higher than NO over both TF0 and P25, indicating that NO_2 would be the preferential product over TiO_2.

3.1.1. Effect of fluorination of TiO_2

As TF4 showed a better performance than other TiO_2, we wonder if the surface F ions have an impact on the photo-oxidation of NH_3 and formation of NO and NO_2. Therefore, we defluorinated TF4 by washing with NaOH (TF4-NaOH) and calcinated at 500 ℃ (T500), respectively, and compared their photocatalytic activity. As seen from Fig. 2(a), the defluorination of TF4 has great influence on NH_3 adsorption and oxidation, following the order: TF4 >TF4-NaOH>T500. It has been reported [39] that the surface defluorination by NaOH could replace the F ions with hydroxyl groups on $TiO_{2\ surface}$, while Ti-OH has a weak interaction with NH_3, leading to an obvious amount of NH_3 desorption at the start of irradiation. During irradiation, NO and NO_2 increased at first 60 min and then stabilized to a steady-state concentration of ~70 ppb and ~300 ppb, respectively, over TF4-NaOH, and 35 ppb, 100 ppb over T500 (Fig. 2(b and c)), far higher than that of TF4 (12 ppb). Therefore, the surface defluorination of TF4 reduced the photocatalytic activity and increased the formation of noxious NO_x. Besides, in order to further clarify the role of surface fluorine on the photocatalytic oxidation of NH_3, we compared the photocatalytic activity of F modified TF0 and P25 (Fig. S2). It turned out that the process of fluorination had no obvious impact on the degradation of NH_3, while it could reduce the formation of NO_x, especially for NO_2. In conclusion, surface fluorination on the TiO_2 might have an influence on the NH_3 photocatalytic oxidation pathways, inhibiting the generation of noxious NO_x.

3.1.2. Effect of Pt deposition

Pt, known as a good electron cocatalyst, was widely used in modification of photocatalysts by efficient trapping of photoexcited electrons, decreasing the combination of photoproduced charge carriers, and consequently improving the photocatalytic oxidation reactions [40,41]. Besides, the Pt deposition would extend the light absorption of TiO_2 to the visible spectrum [38]. In order to figure out whether Pt deposition on TiO_2 would affect the photo-degradation of NH_3, the conversion of NH_3 to NO_x on Pt-loaded TiO_2 (Pt-P25, Pt-TF4, Pt-TF0) was investigated at initial NH_3 concentrations of 820 ppb in Fig. 3. Compared with the bare TiO_2 in Fig. 1, the modification of Pt could remarkably enhance the NH_3 photo-degradation efficiency and reduce the amount of formed NO_x. Among all the catalysts, Pt-TF4 exhibited the best performance on NH_3 conversion with 290 ppb outlet, ~100 ppb less than that of TF4 and Pt-TF0. Fig. 3(b and c) shows that the steady-state NO and NO_2 concentration of Pt-TF4 also remained constant at a very low value of 4 ppb and 3.5 ppb, respectively. However, even the conversion reactivity of NH_3 was close to that of Pt-TF4, Pt-P25 produced 3 times as much NO_x as Pt-TF4, but still much less than bare P25. In addition, the amount of NO_x over Pt-TF0 kept increasing to 80 ppb of NO and 65 ppb of NO_2 during the irradiation. It is worth noted that bare TiO_2 generates much more NO_2 than NO, while Pt-loaded TiO_2 generates more NO, indicating that the process of Pt deposition not only enhanced photocatalytic oxidation activity of NH_3, but also greatly decreased the formation of noxious NO_x, and changed the pathway of NH_3 degradation.

3.1.3. Characterization of catalysts

The SEM and TEM images of the prepared TF4 with various magnifications are shown in Fig. S3. It can be seen that the TiO_2 nanostructures have grown into a rectangular shape with a side length of ~30 nm and thickness of ~4 nm. The free-standing TF4 shows that the nanosheet is well crystallized and the lattice spacing parallel to the top and bottom facets is *ca.* 0.235 nm, corresponding to the (001) planes of anatase TiO_2, confirming that the TF4 has morphology of nanosheets with

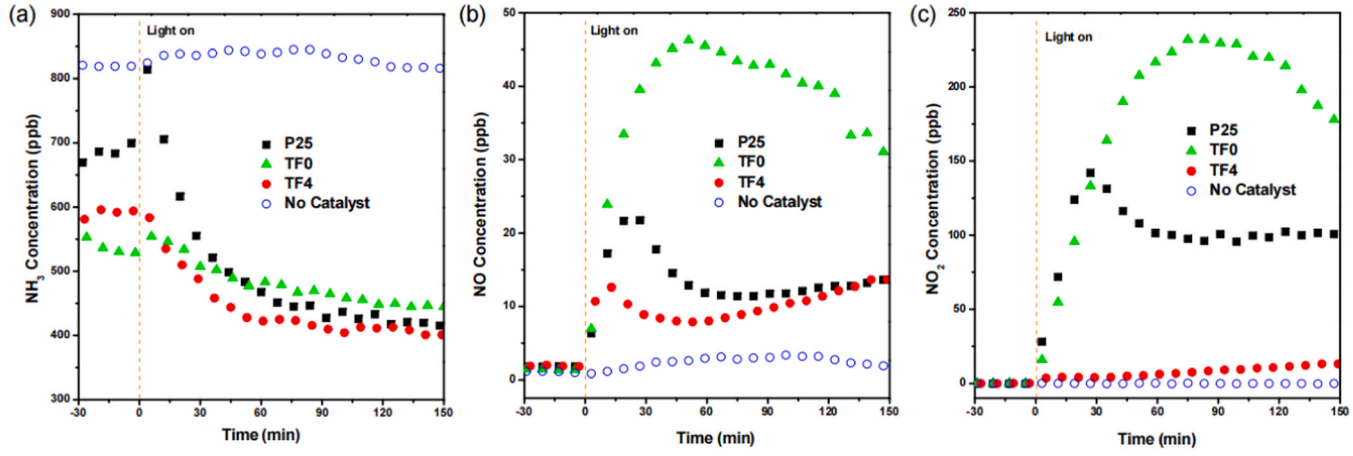

Fig. 1. (a) Outlet NH_3 concentration; (b) Outlet NO concentration; (c) Outlet NO_2 concentration of different samples under simulated sunlight irradiation.

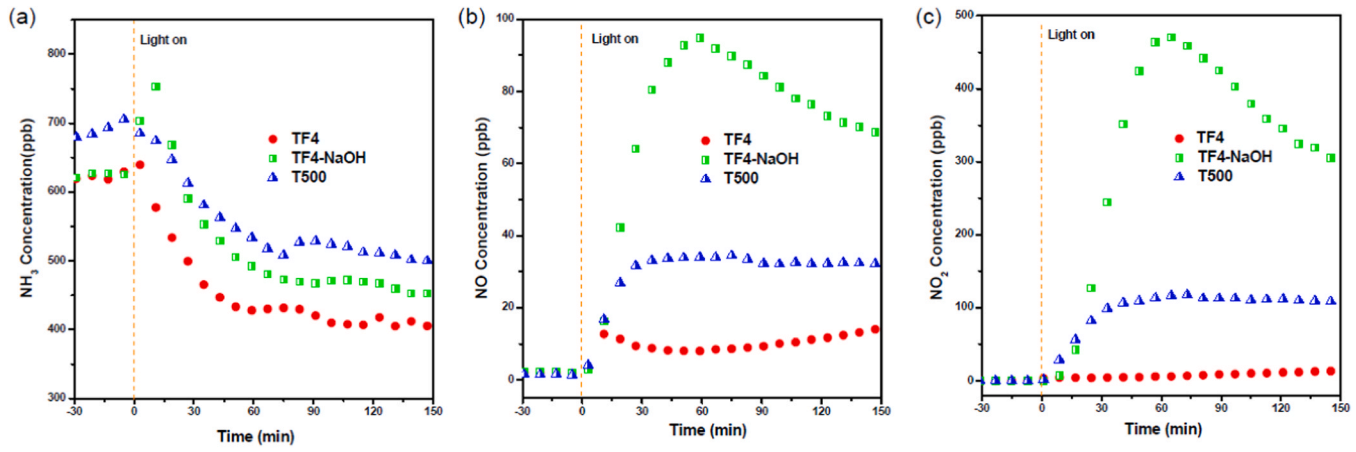

Fig. 2. (a) Outlet NH_3 concentration; (b) Outlet NO concentration; (c) Outlet NO_2 concentration of different samples (TF4, TF4-NaOH and T500) under simulated sunlight irradiation.

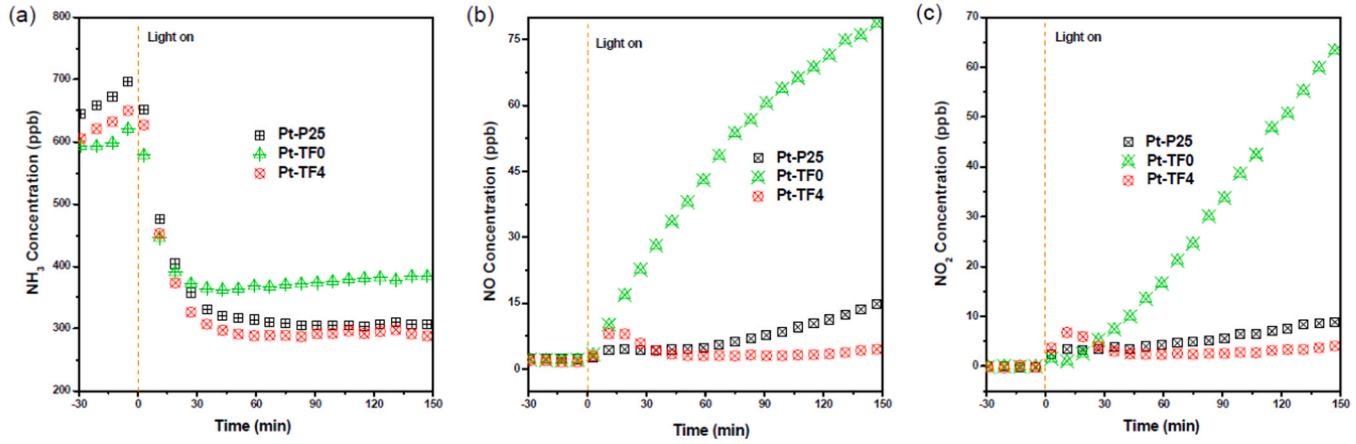

Fig. 3. (a) Outlet NH_3 concentration; (b) Outlet NO concentration; (c) Outlet NO_2 concentration of different samples (Pt-P25, Pt-TF0 and Pt-TF4) under simulated sunlight irradiation.

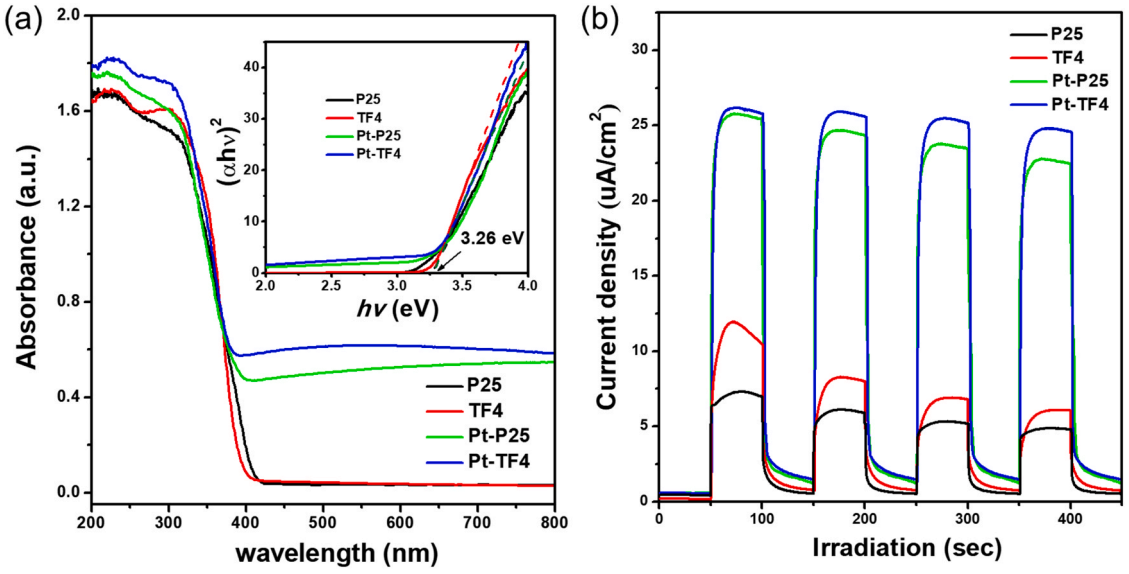

Fig. 4. (a) UV-Vis diffuse reflectance spectra and plots of $(\alpha h\nu)^{1/2}$ *vs.* Photo energy (inset) and (b) The transient response all samples at 0.4 V *vs.* Ag/AgCl electrode.

dominant {001} facets. XRD patterns of TF4 and Pt-TF4 further reveal the formation of pure anatase structure (JCPDS No. 21-1272), where four main diffraction peaks at 2θ of 25.4°, 37.8°, 48.0°, and 55.1° were indexed into to the (101), (004), (200), and (211) of anatase TiO_2, respectively, while P25 and Pt-P25 show peaks both from anatase and rutile phase (Fig. 4c). All the samples display a good crystallinity, but no obvious peaks associated with Pt species were detected in the XRD patterns of Pt-P25 and Pt-TF4. This is possibly ascribed to the low loading amount, weak crystallization and high dispersion of the Pt (1%). Moreover, the loading of Pt by the photodepositoon method induce no significant change in the phase structure of TiO_2. The nitrogen adsorption-desorption isotherms and the corresponding pore-size distribution curves (inset) for P25 and TF4 are also shown in Fig. S3 (d). The isotherms corresponding to TF4 are of type IV (Brunauer-Deming-Deming-Teller (BDDT) classification) with a H_2 hysteresis loop at high relative pressures, indicating the presence of ink-bottle shaped mesopores (2–50 nm) formed between anatase nanosheets. The commercial P25 has a H3-type hysteresis loop, suggesting the presence of slit-like pores. The Brunauer-Emmett-Teller (BET) surface area of TF4 is determined to be 103 $m^2\ g^{-1}$, much higher than that of P25 (43 $m^2\ g^{-1}$).

The optical absorption properties are obtained by the UV-Vis absorption spectroscopy. It can be seen from Fig. 4(a) and inset, both P25 and TF4 show a typical absorbance band onset at *ca.* 400 nm with calculated energy gap of 3.26 eV, corresponding to the intrinsic electron excitation from the valence to the conduction band of anatase TiO_2. After the deposition of Pt, an obvious enhancement in the wavelength absorption of 400–800 nm is observed, indicating the increased light harvesting in the visible range. Besides, no absorption edge shift and energy gap change occurred compared to the pristine TiO_2, further suggesting that Pt is only deposited on the surface of TiO_2 by photodepositon method. The transient photocurrent responses to the on-off cycles under illumination in Fig. 4(b) also demonstrated a noticeable improvement of charge separation efficiency by the introduction of Pt and F. It should be noted that the photocurrent densities of TF4 and Pt-TF4 are higher than that of P25 and Pt-P25, indicating that fluorinated TiO_2 nanosheet show higher charge migration efficiency than P25 due to the synergistic effect of surface fluorination and exposed {001} facets on the photoactivity of TiO_2.

3.2. Photocatalytic mechanism over F modified TiO_2

3.2.1. Role of reactive species

Generally, the potential reactive species involved in the photocatalytic oxidation of NH_3 could be the photogenerated holes (h^+) and electrons (e^-), and formed oxidizing species from them, such as $\bullet O_2^-$, H_2O_2 and •OH. In order to investigate the effects of mentioned reactive species, radical trapping experiments were performed by using sodium oxalate ($Na_2C_2O_4$, h^+ scavenger), potassium dichromate ($K_2Cr_2O_7$, electron scavenger), tert-butyl alcohol (t-BuOH, •OH scavenger), Fe(II)-EDTA (H_2O_2 scavenger) and 2,2,6,6-tetramethylpiperidine-1-oxy (tempo, $\bullet O_2^-$ scavenger), respectively. Taken into account that NH_3 has a strong water absorption and adsorption, we take the generated concentration of NO and NO_2 as the evaluation indexes. As is shown in Fig. 5, compared with the oxidation process without scavengers, the presence of $Na_2C_2O_4$ and $K_2Cr_2O_7$ both obviously suppressed the generation of NO and NO_2 over P25 and TF4, indicating that both h^+ and e^- participate in the NH_3 oxidation into NO and NO_2. Especially for P25, the outlet NO_2 concentration decreased from 100 ppb to 0 ppb, suggesting that the photogenerated h^+ and e^- play an indispensable role in NO_2 generation. However, when t-BuOH and tempo were added, the outlet concentration of both NO and NO_2 increased over P25 and TF4, especially after scavenging of $\bullet O_2^-$, the NO and NO_2 concentration are 3–5 times higher than those without scavenger, indicating that •OH and $\bullet O_2^-$ could depressed the photocatalytic oxidation of NH_3 into NO and NO_2 or facilitate the further conversion of NO to NO_2 and NO_2 to NO_2^- or NO_3^-. As both •OH and $\bullet O_2^-$ are highly reactive oxygenated radical species, the possible pathways for NH_3 photocatalytic oxidation by •OH and $\bullet O_2^-$ might involve the processes of oxidizing NO to NO_2 and oxidizing NO_2 to nitrite and nitrate. The scavenging effect of Fe (II)-EDTA shows a negligible influence on photocatalytic oxidation activity, indicating that H_2O_2 would not be the major reactive species for both P25 and TF4 in this process.

3.2.2. H_3 adsorption and oxidation activity by In-Situ DRIFT

In order to get further insight into the mechanism of NH_3 photocatalytic oxidation over TiO_2 based catalysts (commercial P25 and nanosheet TF4), the NH_3 adsorption and conversion behaviors were investigated by the *in-situ* Diffuse Reflectance Fourier Translation Infrared Spectroscopy (DRIFTS) upon light. As displayed in Fig. 6, P25 and TF4 were first pretreated by being exposed to NH_3 in synthetic air flow for 120 min without illumination. With the introduction of NH_3, several bands on the P25 at 1187 cm^{-1}, 1374 cm^{-1} and 1474 cm^{-1} appeared and its intensity increased with the exposure time, which were the characteristics of the NH_3 adsorbed species over P25. The band at 1187 cm^{-1}, ascribed to the coordinated NH_3 bound to Lewis acid sites, shown a higher enhancement than the bands at 1374 and 1474 cm^{-1} which were assigned to the NH_4^+ on the Brønsted acid sites, suggesting NH_3 was mainly adsorbed on Lewis acid sites over P25. While for TF4, the NH_4^+ species bound to the Brønsted acid sites at 1441 cm^{-1} were much stronger than those of coordinated NH_3 species on Lewis acid sites

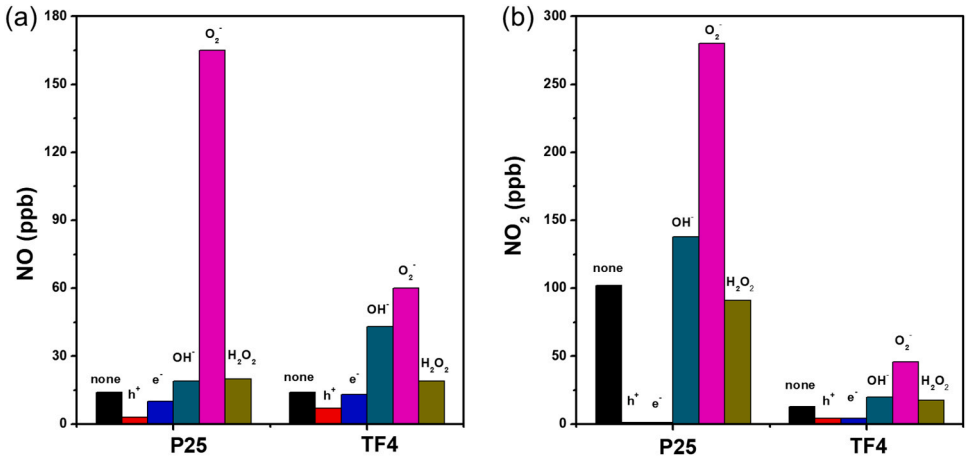

Fig. 5. Scavenger experiments of reactive species during the photocatalytic degradation of NH_3 over P25 and TF4 (a) NO Concentration; (b) NO_2 Concentration under simulated sunlight irradiation.

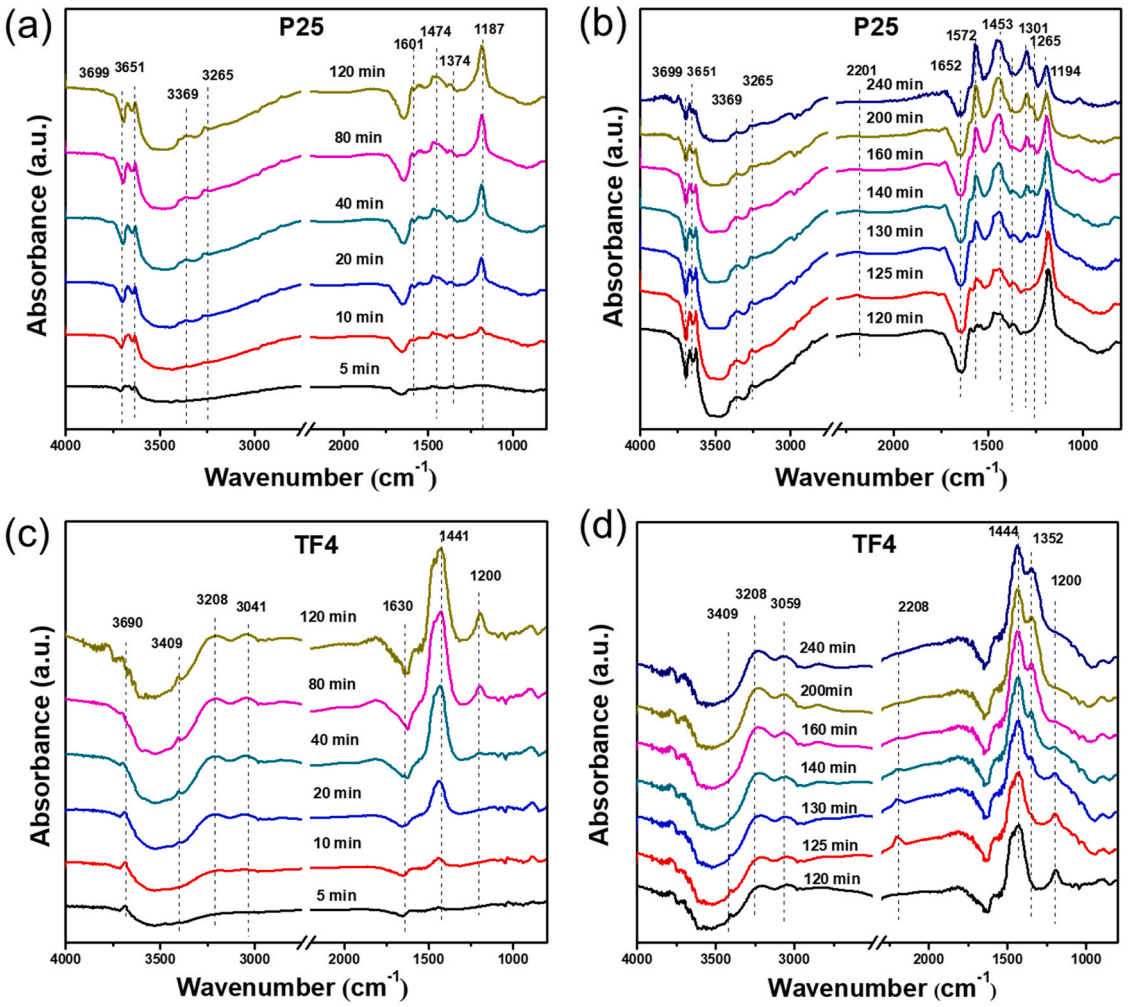

Fig. 6. *In-situ* DRIFTS of (a) NH_3 adsorption process over P25; (b) photocatalytic oxidation process over P25; (c) NH_3 adsorption process over TF4 and (d) photocatalytic oxidation process over TF4 in 120 min.

at 1200 cm^{-1}, indicating that Brønsted acid sites were the main adsorption sites over TF4. Besides, the bands around 3265 and 3369 cm^{-1} can be assigned to N-H stretching vibrations of coordinated NH_3. Noted that the bands around 3651 and 3699 cm^{-1}, which can be attributed to OH stretching vibration of surface hydroxyl groups, together with bands at 1630 cm^{-1} ascribed to the deformation of water, kept increasing with the exposure time due to the RH= 50 in the continuous flow system.

After 120 min of the adsorption of NH_3, the gas flow was switched off and the samples were subsequently irradiated for 120 min. As the photoreaction proceeded, new bands between 1100 and 1700 cm^{-1} and a broad adsorption band between 3000 and 3700 cm^{-1} were detected. Fig. 6(b) shows that NH_3 adsorption both at Lewis acid sites (1194 cm^{-1}, 3265 cm^{-1} and 3369 cm^{-1}) and Brønsted acid sites (1353 cm^{-1}) become weak, suggesting that both NH_4^+ and coordinated NH_3 are involved in the reaction. At the same time, the characteristic bands of nitrate species (NO_3^-) appeared at 1301 cm^{-1} (monodentate nitrates), and 1572 cm^{-1} (bidentate nitrates), co-existing with the band at 1652 cm^{-1} (adsorbed NO_2), meaning that the adsorbed NH_3 species were exhausted and oxidized into NO_x and nitrates. Besides, an enhancement of band at 1453 cm^{-1} assigned to ionic $NH4^+$ which has gradually shifted from higher wavenumber (1474 cm^{-1}) was observed, suggesting the new Brønsted acid sites formed from M-NO_2 nitro compounds (NH_2NO_2) [42]. The small bands at 1265 and 2201 cm^{-1} could be assigned to N_2 and N_2O adsorption on the Lewis acid site, respectively. And N_2O would further dissociate into N_2 and H_2O, indicating that in addition to nitrate and nitro compounds, N_2 can be also generated during the photo-oxidation of NH_3 over commercial TiO_2. Similar products have reappeared over TF4 nanosheet as shown in Fig. 6(d). The intensity of the peaks of the coordinated NH_3 bound to Lewis acid sites at 1200 and 3409 cm^{-1} gradually decreased, while new band appeared at 1352 cm^{-1} due to the free nitrate ions under simulated sunlight irradiation. Besides, the band attributed to the M-NO_2 compounds (1444 cm^{-1}) overlapped the band of ionic NH_4^+ and grew in intensity as the illumination time increased. Moreover, a much stronger peak at 2208 cm^{-1} assigned to N_2O adsorption over TF4 than P25 was observed after photo-irradiating for 5 min, further confirming the generation of N_2 in the process. Compared with those products over P25, more mildly oxidized products like nitrite and N_2 can be formed during the photo-oxidation process of NH_3, which is in accordance with the result that TF4 has a much lower NO and NO_2 outlet concentration than P25.

3.2.3. *XPS analysis*

Since the DRIFTS spectra cannot clearly identify the species formed on catalysts, XPS was used to elucidate the chemical properties of surface-adsorbed species (Fig. 7). For Ti 2p peaks, two main peaks assigned to for Ti 2p3/2 and Ti 2p1/2 are observed on both P25 and TF4, corresponding to Ti4+ reported in TiO2. Compared with the XPS spectra of fresh catalysts, a binding energy shifted to lower value over the commercially available P25 after the reaction (P25-R), while a completely different trend was observed for the binding energies over TF4 after reacting (TF4-R), which indicated a diverse interaction with

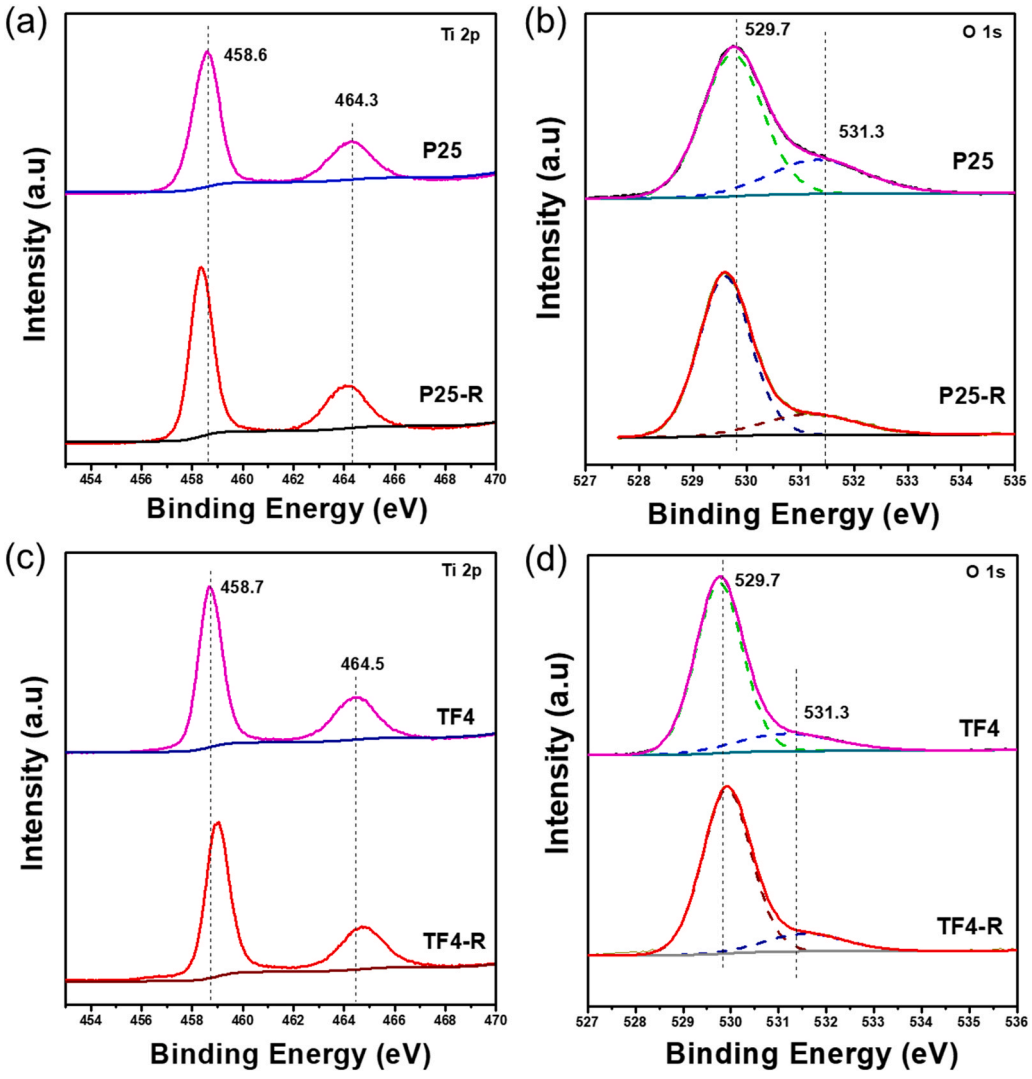

Fig. 7. XPS of P25 (a) Ti 2p; (b) O 1s; of TF4 (c) Ti 2p and (d) O 1s before and after reaction.

NH3 over P25 and TF4 during the photocatalytic oxidation. For O 1s XPS spectra, the same changes for the original binding energies and their reacted counterparts have been observed over P25 and TF4 as well. A shift toward lower binding energy upon reacted P25 indicated that during the interaction with NH3, P25 tended to gain the electrons, while TF4 preferred to lose the electrons due to its weakly oxidized surface state after reaction. This is also confirmed by the XPS spectrum of F 1s region shown in Fig. S4, whose binding energy shifted to higher value on

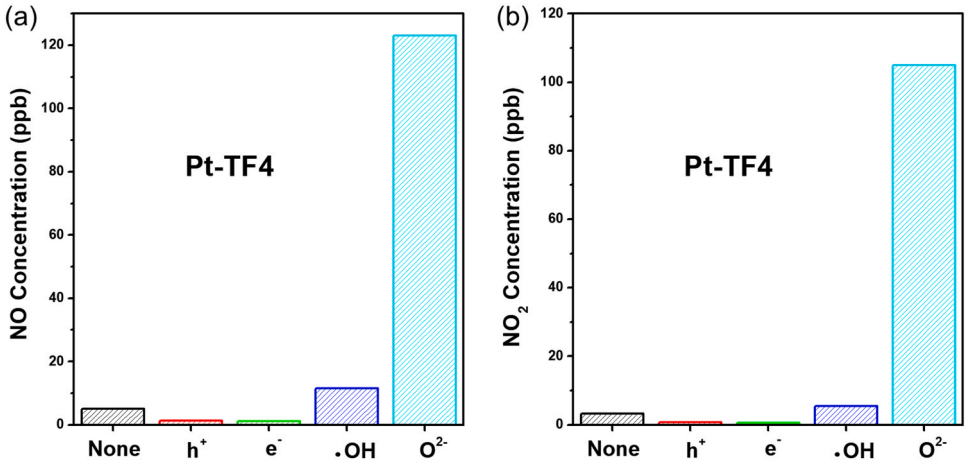

Fig. 8. Scavenger experiments of reactive species during the photocatalytic degradation of NH_3 over Pt-TF4 (a) NO Concentration; (b) NO_2 Concentration simulated sunlight irradiation.

the reacted TF4, indicating that the adsorbed reactants such as NH_3, O_2, NO, NO_2 etc. on TF4 would be partly reduced into mildly oxidized products by obtaining the electrons. The observations of XPS analysis are consistent with the results that only 12 ppb of both NO and NO_2 was formed over TF4 on the photocatalytic oxidation of NH_3 and more N_2 was found in *in-situ* DRIFT spectrum.

3.3. Photocatalytic mechanism over Pt deposited TiO_2

3.3.1. Role of reactive species

As can be seen in Fig. 8, after deposition of Pt, Pt-TF4 has the same trend with TF4 and P25, further confirming that both the photo-generated h^+ and e^- are primarily responsible for oxidizing NH_3 to NO and NO_2, whereas the •OH and $•O_2^-$, especially $•O_2^-$ would play a critical role in enabling further oxidation of NO and NO_2. Compared with Figs. 5 and 8, it should be noted that the influence of $•O_2^-$ over TF4 are much weaker than that over P25 and Pt-TF4, indicating that TF4 would have a different NH_3 oxidation mechanism.

3.3.2. NH_3 adsorption and oxidation activity by In-Situ DRIFT

Similar reaction processes reappeared in the DRIFT spectra of Pt-loaded catalysts under the same reaction conditions. As is shown in Fig. 9, several bands due to coordinated NH_3 (1182–1187 and 1557 cm^{-1}) and NH_4^+ (1447–1474 cm^{-1}) on both Pt-P25 and Pt-TF4 were detected and much stronger than that on bare P25 and TF4 after the exposure of NH_3 for 120 min, indicating a stronger adsorption of NH3 by the addition of Pt. Under the irradiation, the main surface adsorbed NH_3 on the catalysts transformed to nitrates and nitrites with different configurations. For Pt-P25, the nitrates species including bidentate nitrate (1045 cm^{-1}) and monodentate nitrates (1307 cm^{-1}), together with adsorbed NO_2 and M-NO_2 (1655 and 1457 cm^{-1}) were generated during the photoreaction process. Besides, the small bands at 2200 cm−1 due to N_2O adsorption also suggested the production of N_2 over Pt-P25. The *in-situ* DRIFT spectra over Pt-TF4 was similar to that over Pt-P25. Obvious enhancement of bidentate nitrate (1032 and 1581 cm^{-1}), monodentate nitrates (1300 cm^{-1}) and M-NO2 (1440 cm^{-1}) were found over Pt-TF4 under irradiation. And the amount of formed NO_x and nitrates species on both Pt-P25 and Pt-TF4 were much larger than on bare P25 and TF4, which could be attributed to the stronger redox ability.

3.3.3. XPS analysis

After the deposition of Pt, both Pt-P25 and Pt-TF4 showed the similar trends with P25 in Fig. 10. All the Ti 2p, O 1s and Pt 4f binding energies shifted to lower value after the reaction, revealing that the surface of catalysts was slightly reduced and the adsorbed reactants were being oxidized during the photo-oxidation of NH_3. In combination with the results that Pt-loaded TiO_2 generated much less NO_x than bare TiO_2 in the degradation of NH_3 and more nitrates species were observed in *in-situ* DRIFT spectrum, we can deduce that the deposition of Pt would significantly enhance the photocatalytic performance of TiO_2 by suppressing the migration of photo-generated electrons and may further

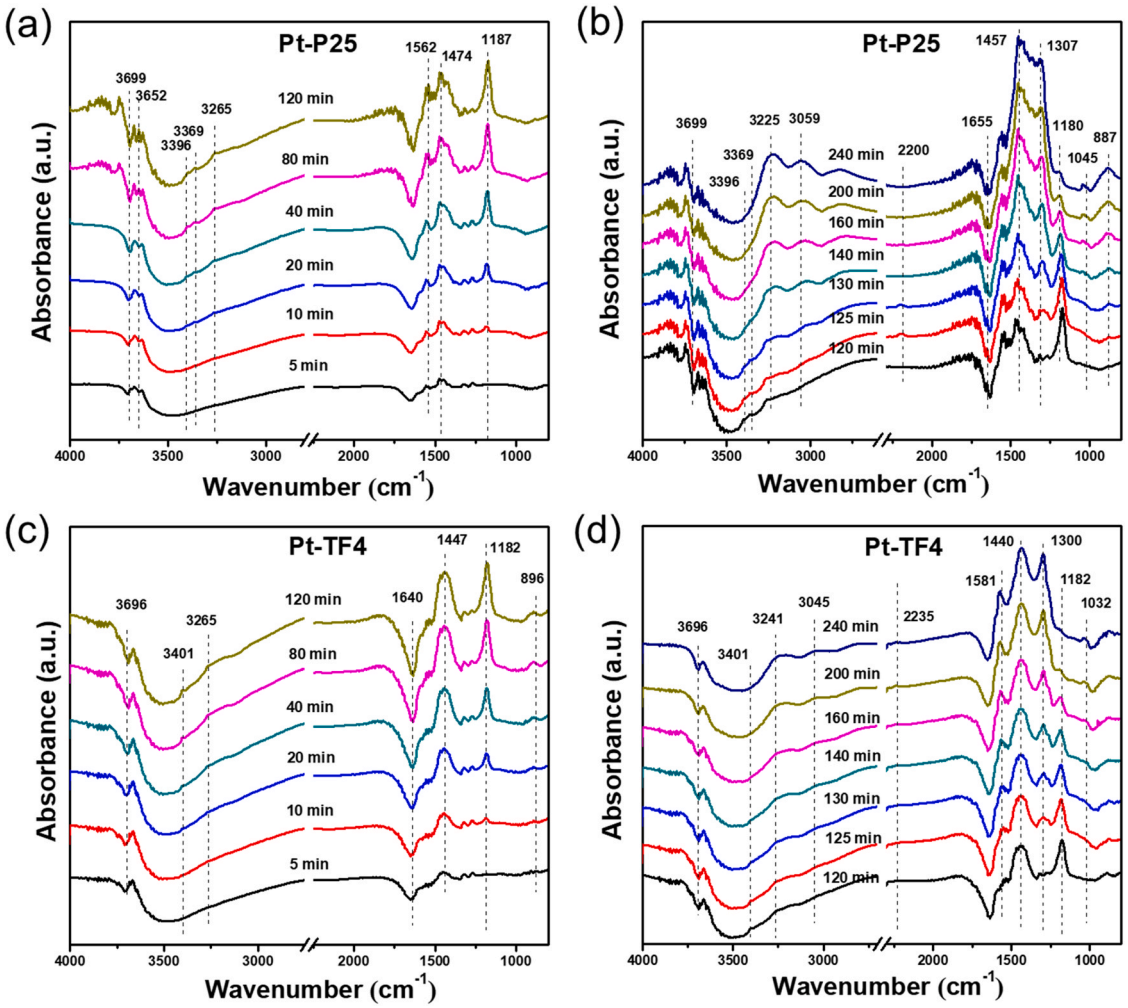

Fig. 9. *In-situ* DRIFTS of (a) NH_3 adsorption process; (b) photocatalytic oxidation process over Pt-P25; (c) NH_3 adsorption process and (d) photocatalytic oxidation process over Pt-TF4 in 120 min.

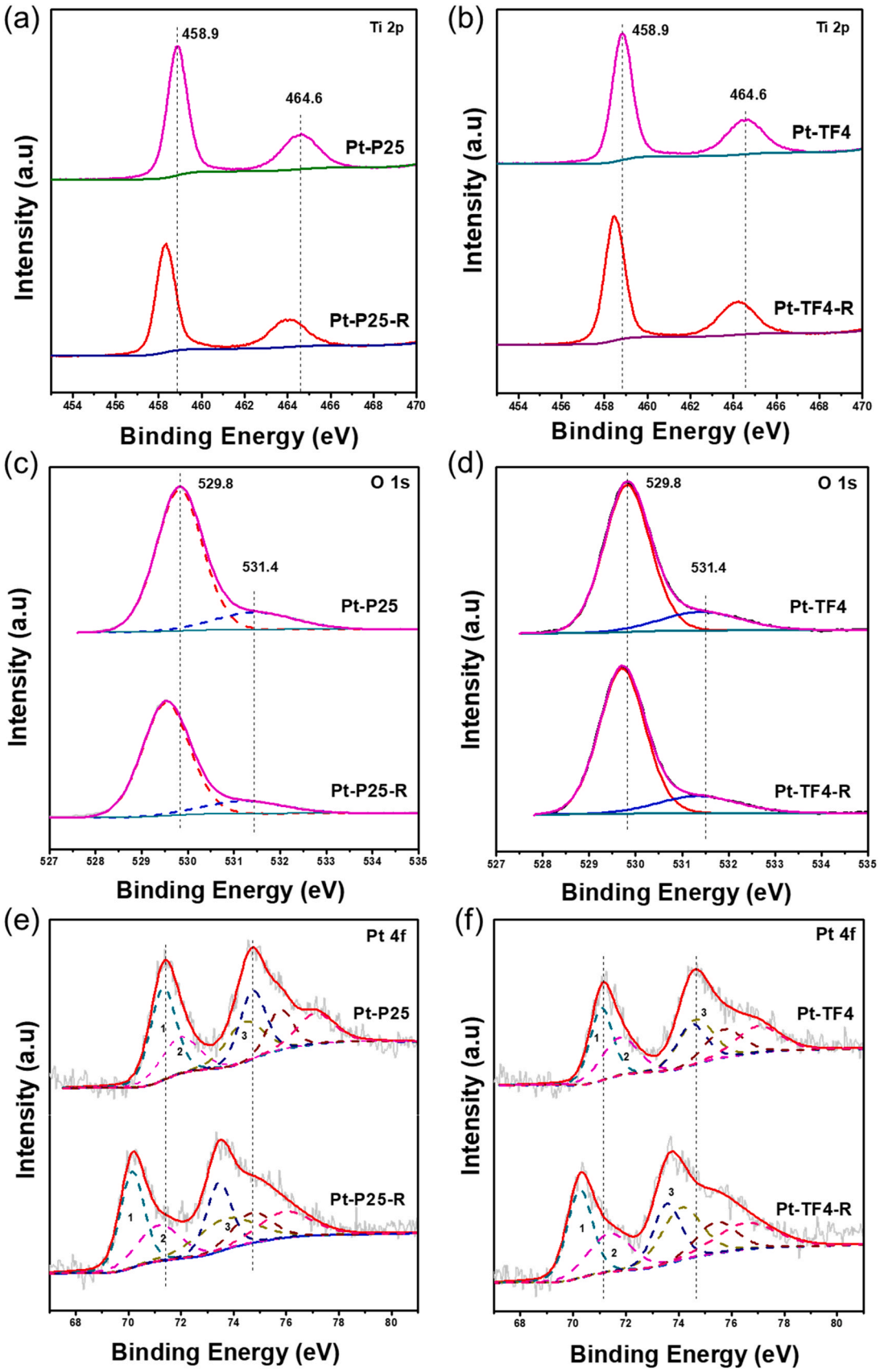

Fig. 10. XPS spectrum of (a~b) Ti 2p, (c~d) O 1s and (e~f) Pt 4f over Pt-P25 and Pt-TF4 before and after reaction.

oxidize formed NO_x into nitrates species. It should be noted that the F1s peaks at ~684 eV (Fig. S4) were attributed to Ti-F bound, suggesting the presence of surface fluorine on both TF4 and Pt-TF4. Besides, the XPS spectrum of high-resolution Pt 4 f showed that Pt-P25 and Pt-TF4 had two obvious peaks of Pt 4f7/2 and 4f5/2 at 71.4 and 74.8 eV, respectively, indicating the existence of the multivalence Pt and Pt can be partly reduced by photodeposition method. The binding energy peaks of N 1s for all the samples after reaction were shown in Fig. S4. For P25 and TF4, only one peak centered at 399.8 eV and 401.3 eV, corresponding to coordinated NH_3 bound to Lewis acid sites and NH_4^+ bound to the Brønsted acid sites, respectively. While for Pt-TF4, a peak at higher binding energy 406.5 eV, can be attributed to the adsorbed nitrates, which was in accordance with the *in-situ* DRIFT results. It should be noted that the adsorption of NH_3 on TiO_2 is stronger than that of NO_x species as NO_x species is not easily adsorbed on TiO_2 where NH_3 is already there.

4. Discussion

Based upon the results of *in-situ* DRIFT and XPS analysis, the following reaction steps are suggested here as a plausible mechanism for the photocatalytic oxidation of NH_3 on TiO_2 based photocatalysts (Fig. 11). The initial step of NH_3 oxidation is the adsorption of NH_3 as coordinated NH_3 bound to Lewis acid sites and NH_4^+ bound to the Brønsted acid sites on TiO_2. Then the disappearance of the bands of coordinated NH_3 under simulated sunlight irradiation shown in Figs. 6 and 9 strongly indicate that NH_3 was the major activated form and the adsorbed NH_3 collide with a valence band hole on the TiO_2 surface, leading to the formation of reactive amino radical (Eq. 4). The formed $\bullet NH_2$ has been observed by electron paramagnetic resonance (EPR) spectroscopy and believed to be a critical intermediate in previous studies[43,44] of NH_3 oxidation on TiO_2. $\bullet NH_2$ could react with O_2, $\bullet O_2^-$ and $\bullet OH$ generated on TiO_2 based photocatalysts under light irradiation (Eqs. 2 and 3), leading to the production of NO_x (including NO and NO_2) (Eqs. 5 and 6), and further oxidation to NO_2^- and NO_3^- (Eqs. 7–9). The formed NOx species then react with $\bullet NH_2$ or NH_3 to produce N_2 via NH_2NO as an intermediate over TiO_2 under illumination (Eq. 14). Besides, NO_2 has been reported [45] to be more active than NO to react with NH_3 to give N_2 or N_2O.

$$TiO_2 + h\nu \rightarrow e_{cb}^- + h_{vb}^+ \quad (1)$$

$$O_2 + e_{cb}^- \rightarrow \bullet O_2^- \quad (2)$$

$$H_2O + h_{vb}^+ \rightarrow \bullet OH + H^+ \quad (3)$$

$$NH_3 + h_{vb}^+ \rightarrow \bullet NH_2 + H^+ \quad (4)$$

$$\bullet NH_2 + O_2 \rightarrow NO + H_2O \quad (5)$$

$$2NO + O_2 \rightarrow 2NO_2 \quad (6)$$

$$\bullet NH_2 + \bullet O_2^- \rightarrow NO^- + H_2O \quad (7)$$

$$2NO^- + O_2 \rightarrow 2NO_2^- \quad (8)$$

$$NO^- + O_2 \rightarrow NO_3^- \quad (9)$$

$$NO_2 + \bullet O_2^- \rightarrow NO_2^- + O_2 \quad (10)$$

$$NO_2^- + \bullet OH \rightarrow HOONO \rightarrow NO_3^- + H^+ \quad (11)$$

$$NO_2^- + H_3O^+ \rightarrow HONO + H_2O \quad (12)$$

$$NH_3 + HONO \rightarrow NH_4NO_2 \rightarrow N_2 + 2H_2O \quad (13)$$

$$\bullet NH_2 + NO \rightarrow NH_2NO \rightarrow N_2 + H_2O \quad (14)$$

$$\bullet NH_2 + NO_2 \rightarrow NH_2NO_2 \rightarrow N_2 + H_2O + O_2 \text{ (or } 2O_{ads}) \quad (15)$$

$$NH_4^+ + NO_3^- \rightarrow NH_4NO_3\ (h\nu) \rightarrow N_2 + 2H_2O + O_{ads} \quad (16)$$

TF4 has shown less production of NO_2 and NO compared to P25 and TF0 and our above results indicate that the process of fluorination could reduce the formation of NO_x, especially for NO_2. The promoting effect of fluorine on catalytic selectivity of oxidation pathways could be attributed to the strong electron- trapping ability with electronegativity [46], which could hinder the recombination of photo-generated electrons and holes, and enhance the formation of $\bullet NH_2$, $\bullet O_2^-$ and $\bullet OH$ on TiO_2 nanosheets. He et al. [34] also found a remarkable synergistic effect between fluorine and {001} facets on the photogenerated hole

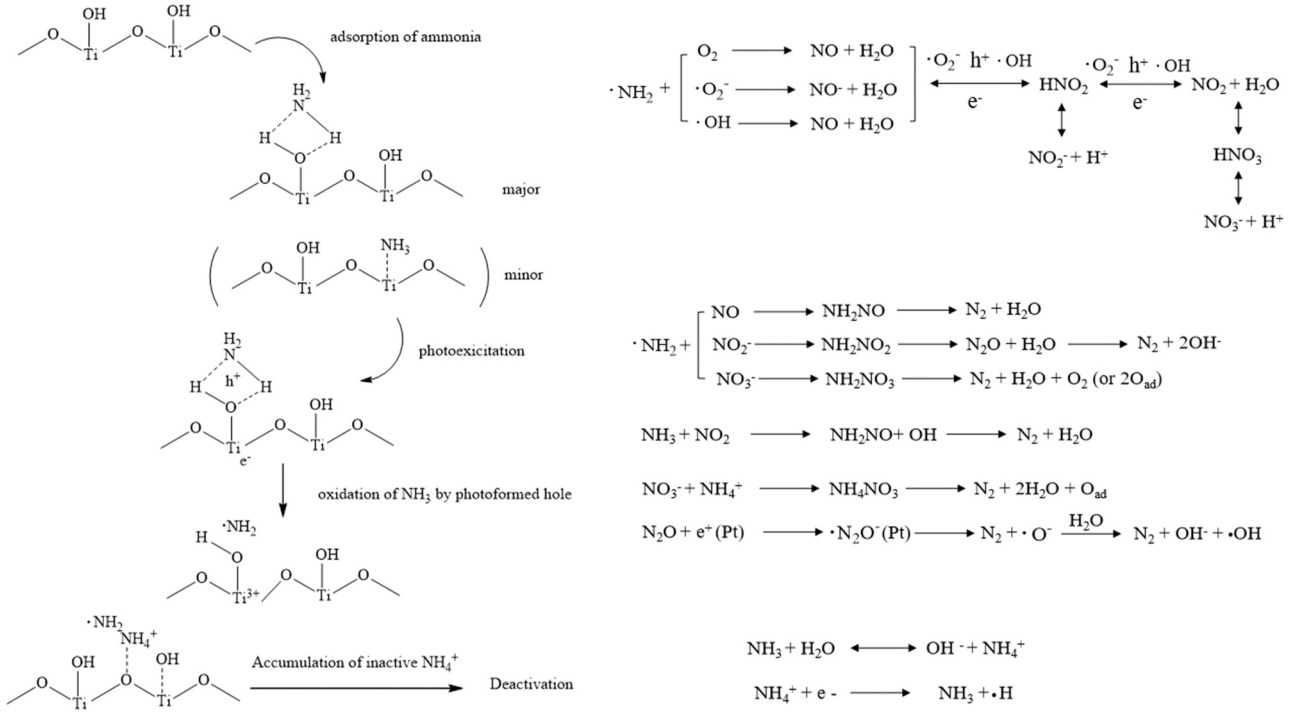

Fig. 11. Proposed mechanism of Photocatalytic degradation process of ammonia under simulated sunlight irradiation.

migration, which can significantly promote the enhance the photo oxidation of NH_3. In addition, surface fluorination can significantly enhance the adsorption of NH3 on the TiO_2 surface [31,47], leading to the generation of NO_x. Those NO_x species can immediately react with other unreacted NH_3 adsorbed on TiO_2. However, for those TiO_2 without fluorine, like P25 and TF0, the amount of adsorbed NH_3 is small, the formed NO_x species can hardly react with NH_3 but to accumulate on the TiO_2 surface. Deposition of Pt could further extend the lifetime of the electron–hole pairs by strongly capture the electron, and hence enhance the availability of holes migrated to the surface of TiO_2 as oxidative sites and electrons migrated to electron-rich Pt as reductive sites, which may donate electrons to NO_x and thereby promote the generation of N_2. Choi et al. [48] proposed that Pt depositing on TiO_2 could enable the selective oxidation of NH_3 to N_2 by trapping electrons and reductively dissociating formed N_2O into N_2 and •OH. However, based on our *in-situ* DRIFT and XPS analysis, a large amount of nitrates and nitrites is formed on Pt-based TiO_2, and after the photo-oxidation of NH_3 Pt-based TiO_2 was slightly reduced, indicating that the deposition of Pt on TiO_2 could significantly enhance the photocatalytic performance by generating reactive $•O_2^-$ (Eq. 2) (confirmed by the our scavenger experiments above) and further oxidize formed NO_x into nitrates and nitrites species. It should be noted that this selective photocatalytic oxidation of NH_3 to N_2 is believed to be applicable only to NH_3, not to NH_4^+, but NH_4^+ can be reduced to NH_3 or react with NO_2 to produce N_2 via NH_4NO_2 intermediate under UV irradiation (Eq. 16).

5. Conclusions

In summary, we have developed F and Pt modified TiO_2 to improve photocatalytic activity toward NH_3 oxidation and suppress the formation of harmful products such as NO and NO_2. Results showed a promoting effect and synergistic effect for both Pt deposition and surface F ions modification on the mild oxidation of NH_3 into N_2. Surface fluorination can reduce the generation of noxious NO_x, especially for NO_2 due to the enhanced adsorption of NH_3 and the strong electron-trapping ability to retard the recombination of photo-generated electrons and holes. And the trapped electron can be used to reduce the formed NO_x into N_2. Pt deposition can also extend the lifetime of the electron–hole pairs by strongly capture the electron, and enhance the degradation of NH_3. According to the *in-situ* DRIFT and XPS analysis, more nitrates and nitrites are formed on Pt-based TiO_2, showing a different oxidation mechanism by generating more reactive oxygen species ($O_2 + e^- \rightarrow •O_2^-$) and improving the photocatalytic oxidation ability. This work provides fundamental and novel insights for the photocatalytic oxidation of NH_3 on TiO_2 based catalysts, and can be extend to other metal oxide with surface modification to develop “self-cleaning” surfaces for future air pollution removal.

CRediT authorship contribution statement

Yajie Shu: Investigation, Writing – original draft. **Jian Ji** and **Ming Zhou**: Writing - editing & proofreading. **Shimin Liang**, **Quan Xie**, **Sitan Li**, and **Biyuan Liu**: Assist in experimental tests. **Jiguang Deng** and **Jianping Cao**: review & editing. **Shengwei Liu** and **Haibao Huang**: Conceptualization, Supervision, Writing – review & editing, Funding acquisition.

Declaration of Competing Interest

The authors declare that they have no known competing financial interests or personal relationships that could have appeared to influence the work reported in this paper.

Acknowledgements

This work is financially supported by the National Natural Science Foundation of China (NSFC) (No. 22076224, 51572209 and 51872341), Fundamental Research Funds for the Central Universities (20lgjc03 and 19lgzd29), the Tip-top Scientific and Technical Innovative Youth Talents of Guangdong Special Support Program (2019TQ05L196 and 2019TQ05L143), the Science and Technology Planning Project of Guangdong Province (2020A0505100033 and 2021A1515010147) and Open Fund of Guangdong Provincial Engineering Laboratory for Air Pollution Control and Guangdong Key Laboratory of Water and Air Pollution Control.

Appendix A. Supporting information

Supplementary data associated with this article can be found in the online version at doi:10.1016/j.apcatb.2021.120688.

References

[1] B. Gu, M.A. Sutton, S.X. Chang, Y. Ge, J. Chang, Agricultural ammonia emissions contribute to China’s urban air pollution, Front. Ecol. Environ. 12 (2014) 265–266.
[2] K.L. Huang, C.C. Liu, C.W. Lee, C.Y. Ma, T.C. Lin, J.H. Tsai, S.J. Chen, Release reductions of gaseous ammonia and nitrogen oxides from electrochemical treatment of swine wastewater, Aerosol Air Qual. Res. 19 (2019) 2490–2501.
[3] Y. Chang, Z. Zou, Y. Zhang, C. Deng, J. Hu, Z. Shi, A.J. Dore, J.L. Collett Jr., Assessing contributions of agricultural and nonagricultural emissions to atmospheric ammonia in a Chinese megacity, Environ. Sci. Technol. 53 (2019) 1822–1833.
[4] T. Liu, X. Wang, B. Wang, X. Ding, W. Deng, S. Lü, Y. Zhang, Emission factor of ammonia (NH_3) from on-road vehicles in China: tunnel tests in urban Guangzhou, Environ. Res. Lett. 9 (2014), 064027.
[5] C. Huang, Q. Hu, S. Lou, J. Tian, R. Wang, C. Xu, J. An, H. Ren, D. Ma, Y. Quan, Y. Zhang, L. Li, Ammonia emission measurements for light-duty gasoline vehicles in China and implications for emission modeling, Environ. Sci. Technol. 52 (2018) 11223–11231.
[6] H. Schwartz-Narbonne, S.H. Jones, D.J. Donaldson, Indoor lighting releases gas phase nitrogen oxides from indoor painted surfaces, Environ. Sci. Technol. Lett. 6 (2019) 92–97.
[7] B. Beck-Friis, S. Smårs, H. Jönsson, H. Kirchmann, SE-structures and environment: gaseous emissions of carbon dioxide, ammonia and nitrous oxide from organic household waste in a compost reactor under different temperature regimes, J. Agr. Eng. Res. 78 (2001) 423–430.
[8] X. Fu, S. Wang, J. Xing, X. Zhang, T. Wang, J. Hao, Increasing ammonia concentrations reduce the effectiveness of particle pollution control achieved via SO_2 and NO_x emissions reduction in East China, Environ. Sci. Technol. Lett. 4 (2017) 221–227.
[9] Y. Wu, B. Gu, J.W. Erisman, S. Reis, Y. Fang, X. Lu, X. Zhang, $PM_{2.5}$ pollution is substantially affected by ammonia emissions in China, Environ. Pollut. 218 (2016) 86–94.
[10] M. Zhao, S. Wang, J. Tan, Y. Hua, D. Wu, J. Hao, Variation of urban atmospheric ammonia pollution and its relation with $PM_{2.5}$ chemical property in winter of Beijing, China, Aerosol Air Qual. Res. 16 (2016) 1390–1402.
[11] W. Yang, H. He, Q. Ma, J. Ma, Y. Liu, P. Liu, Y. Mu, Synergistic formation of sulfate and ammonium resulting from reaction between SO_2 and NH_3 on typical mineral dust, Phys. Chem. Chem. Phys. 18 (2016) 956–964.
[12] E. Stokstad, Air pollution. Ammonia pollution from farming may exact hefty health costs, Science 343 (2014) 238.
[13] R. Bleizgys, I. Bagdoniene, Control of ammonia air pollution through the management of thermal processes in cowsheds, Sci. Total Environ. 568 (2016) 990–997.
[14] P.N. Bhandari, A. Kumar, R.L. Huhnke, Simultaneous removal of toluene (Model Tar), NH_3, and H_2S, from biomass-generated producer gas using biochar-based and mixed-metal oxide catalysts, Energ. Fuels 28 (2014) 1918–1925.
[15] S. Sommer, E. Jensen, J. Schjørring, Leaf Absorption of Gaseous Ammonia after Application of Pig Sherry on Sand between Rows of Winter Wheat, Joint Workshop COST 611/Working Party 3 and EUROTRAC E. Guyot 1992 395 402.
[16] J.A. Joshi, J.A. Hogan, R.M. Cowan, P.F. Strom, M.S. Finstein, Biological removal of gaseous ammonia in biofilters: space travel and earth-based applications, J. Air Waste Manag. Assoc. 50 (2000) 1647–1654.
[17] H. Kobayashi, A. Hayakawa, K.K.A. Somarathne, E.C. Okafor, Science and technology of ammonia combustion, Proc. Combust. Inst. 37 (2019) 109–133.
[18] P. Bhattacharya, Z.M. Heiden, E.S. Wiedner, S. Raugei, N.A. Piro, W.S. Kassel, R. M. Bullock, M.T. Mock, Ammonia oxidation by abstraction of three hydrogen atoms from a Mo-NH_3 complex, J. Am. Chem. Soc. 139 (2017) 2916–2919.
[19] M. Lin, B. An, N. Niimi, Y. Jikihara, T. Nakayama, T. Honma, T. Takei, T. Shishido, T. Ishida, M. Haruta, T. Murayama, Role of the acid site for selective catalytic oxidation of NH_3 over Au/Nb_2O_5, ACS Catal. 9 (2019) 1753–1756.
[20] Y. Yu, J. Zhao, Y. Yan, X. Han, H. He, A cyclic reaction pathway triggered by ammonia for the selective catalytic reduction of NO_x by ethanol over Ag/Al_2O_3, Appl. Catal. B 136–137 (2013) 103–111.
[21] L.V. Trandafilović, O. Mihai, J. Woo, K. Leistner, M. Stenfeldt, L. Olsson, A kinetic model for SCR coated particulate filters-effect of ammonia-soot interactions, Appl. Catal. B 241 (2019) 66–80.

[22] K. Guo, J. Ji, W. Song, J. Sun, C. Tang, L. Dong, Conquering ammonium bisulfate poison over low-temperature NH_3-SCR catalysts: a critical review, Appl. Catal. B: Environ. 297 (2021), 120388.
[23] H. Morranega, J. Herrmann, P. Pichat, NH_3 Oxidation over UV-irradiated TiO_2 at room temperature, J. Phys. Chem. 83 (1979) 2251–2255.
[24] H. Ou, C. Liao, Y. Liou, J. Hong, S. Lo, Photocatalytic oxidation of aqueous ammonia over microwave-induced titanate nanotubes, Environ. Sci. Technol. 42 (2008) 4507–4512.
[25] K. Obata, K. Kishishita, A. Okemoto, K. Taniya, Y. Ichihashi, S. Nishiyama, Photocatalytic decomposition of NH3 over TiO_2 catalysts doped with Fe, Appl. Catal. B 160–161 (2014) 200–203.
[26] A. Utsunomiya, A. Okemoto, Y. Nishino, K. Kitagawa, H. Kobayashi, K. Taniya, Y. Ichihashi, S. Nishiyama, Mechanistic study of reaction mechanism on ammonia photodecomposition over Ni/TiO_2 photocatalysts, Appl. Catal. B 206 (2017) 378–383.
[27] M. Altomare, M.V. Dozzi, G.L. Chiarello, A. Di Paola, L. Palmisano, E. Selli, High activity of brookite TiO_2 nanoparticles in the photocatalytic abatement of ammonia in water, Catal. Today 252 (2015) 184–189.
[28] S. Yamazoe, T. Okumura, T. Tanaka, Photo-oxidation of NH_3 over various TiO_2, Catal. Today 120 (2007) 220–225.
[29] M.A. Kebede, M.E. Varner, N.K. Scharko, R.B. Gerber, J.D. Raff, Photooxidation of ammonia on TiO_2 as a source of NO and NO_2 under atmospheric conditions, J. Am. Chem. Soc. 135 (2013) 8606–8615.
[30] S. Karapati, T. Giannakopoulou, N. Todorova, N. Boukos, D. Dimotikali, C. Trapalis, Eco-efficient TiO_2 modification for air pollutants oxidation, Appl. Catal. B 176–177 (2015) 578–585.
[31] R. Zhang, Q. Zhong, W. Zhao, L. Yu, H. Qu, Promotional effect of fluorine on the selective catalytic reduction of NO with NH_3 over CeO_2-TiO_2 catalyst at low temperature, Appl. Surf. Sci. 289 (2014) 237–244.
[32] Y. Li, Z. Chen, S. Bao, M. Wang, C. Song, S. Pu, D. Long, Ultrafine TiO_2 encapsulated in nitrogen-doped porous carbon framework for photocatalytic degradation of ammonia gas, Chem. Eng. J. 331 (2018) 383–388.
[33] S. Deng, T. Meng, B. Xu, F. Gao, Y. Ding, L. Yu, Y. Fan, Advanced MnO_x/TiO_2 catalyst with preferentially exposed anatase {001} facet for low-temperature SCR of NO, ACS Catal. 6 (2016) 5807–5815.
[34] M. Chen, J. Ma, B. Zhang, G. He, Y. Li, C. Zhang, H. He, Remarkable synergistic effect between {001} facets and surface F ions promoting hole migration on anatase TiO_2, Appl. Catal. B 207 (2017) 397–403.
[35] R. Wunsch, C. Schön, M. Frey, D. Tran, S. Proske, T. Wandrey, M. Kalogirou, J. Schäffner, Detailed experimental investigation of the NOx reaction pathways of three-way catalysts with focus on intermediate reactions of NH_3 and N_2O, Appl. Catal. B: Environ. 272 (2020), 118937.
[36] M.A. Kebede, N.K. Scharko, L.E. Appelt, J.D. Raff, Formation of nitrous acid during ammonia photooxidation on TiO_2 under atmospherically relevant conditions, J. Phys. Chem. Lett. 4 (2013) 2618–2623.
[37] J. Yu, J. Low, W. Xiao, P. Zhou, M. Jaroniec, Enhanced photocatalytic CO_2-reduction activity of anatase TiO_2 by coexposed {001} and {101} facets, J. Am. Chem. Soc. 136 (2014) 8839–8842.
[38] J. Yu, M. Jaroniec, Hydrogen production by photocatalytic water splitting over Pt/TiO_2 nanosheets with exposed (001) facets, J. Phys. Chem. C 114 (2010) 13118–13125.
[39] H. Wu, J. Ma, Y. Li, C. Zhang, H. He, Photocatalytic oxidation of gaseous ammonia over fluorinated TiO_2 with exposed (001) facets, Appl. Catal. B 152–153 (2014) 82–87.
[40] W. Fang, Z. Qin, J. Liu, Z. Wei, Z. Jiang, W. Shangguan, Photo-switchable pure water splitting under visible light over nano-Pt@P25 by recycling scattered photons, Appl. Catal. B 236 (2018) 140–146.
[41] A.A. Ismail, D.W. Bahnemann, Mesostructured Pt/TiO_2 nanocomposites as highly active photocatalysts for the photooxidation of dichloroacetic acid, J. Phys. Chem. C 115 (2011) 5784–5791.
[42] H. Zheng, W. Song, Y. Zhou, S. Ma, J. Deng, Y. Li, J. Liu, Z. Zhao, Mechanistic study of selective catalytic reduction of NO_x with NH_3 over Mn-TiO_2: a combination of experimental and DFT study, J. Phys. Chem. C 121 (2017) 19859–19871.
[43] S. Yamazoe, K. Teramura, Y. Hitomi, T. Shishido, T. Tanaka, Visible light absorbed NH_2 species derived from NH_3 adsorbed on TiO_2 for photoassisted selective catalytic reduction, J. Phys. Chem. C 111 (2007) 14189–14197.
[44] S. Yamazoe, T. Okumura, Y. Hitomi, T. Shishido, T. Tanaka, Mechanism of photo-oxidation of NH_3 over TiO_2: fourier transform infrared study of the intermediate species, J. Phys. Chem. C. 111 (2007) 11077–11085.
[45] X. Zhao, X. Li, Z. Liu, W. Mu, J. Zhu, L. Su, Z. Li, W. Huang, Insights into the mechanism for the selective catalytic reduction of NO_x with NH_3 on $(MnO)^{2+}$/ZSM-5: a DFT study, J. Theor. Comput. Chem. 16 (2017), 1750030.
[46] H. Park, W. Choi, Effects of TiO_2 surface fluorination on photocatalytic reactions and photoelectrochemical behaviors, J. Phys. Chem. B 108 (2004) 4086–4093.
[47] H. Liu, K.M. Liew, C. Pan, The role of F-dopants in adsorption of gases on anatase TiO_2 (001) surface: a first-principles study, RSC Adv. 4 (2014) 35928–35942.
[48] J. Lee, H. Park, W. Choi, Selective photocatalytic oxidation of NH_3 to N_2 on platinized TiO_2 in water, Environ. Sci. Technol. 36 (2002) 5462–5468.
[49] M. Zhou, T. Li, P. Liu, S. Zhang, Y. Liu, T. An, H. Zhao, Real-time on-site monitoring of soil ammonia emissions using membrane permeation-based sensing probe, Environmental Pollution 289 (2021), 117850.